International Journal of Heat and Mass Transfer 236 (2025) 126334

Contents lists available at ScienceDirect

International Journal of Heat and Mass Transfer

journal homepage: www.elsevier.com/locate/ijhmt

Numerical and geometric investigation of pool boiling heat transfer in cavities with isothermal rectangular corrugations

Gabryell Malcher Freire [a], Cesare Biserni [b], Claudia Naldi [b,*], Felipe Roman Centeno [c], Liércio André Isoldi [a,d], Luiz Alberto Oliveira Rocha [a,c,d,f], Cícero Coelho de Escobar [e], Elizaldo Domingues dos Santos [a,d,f]

[a] Graduate Program of Computational Modeling, School of Engineering, Universidade Federal do Rio Grande, Italia Avenue, km 8 96201-900, Rio Grande, Brazil
[b] Department of Industrial Engineering (DIN), Alma Mater Studiorum – University of Bologna, Viale Risorgimento 2 40136, Bologna, Italy
[c] Graduate Program of Mechanical Engineering, School of Engineering, Universidade Federal do Rio Grande do Sul, Sarmento leite St., 425 90040-001, Porto Alegre, Brazil
[d] Graduate Program of Ocean Engineering, School of Engineering, Universidade Federal do Rio Grande, Italia Avenue, km 8 96201-900, Rio Grande, Brazil
[e] Environmental Science Graduate Program, Engineering Center, Universidade Federal de Pelotas, Benjamin Constant Street, 989 96010-020, Pelotas, Brazil
[f] Complex Fluid Systems Lab, Institute of Earth Sciences, Rua Romao Ramalho 59 7000-671 Evora, Portugal

ARTICLE INFO

Keywords:
Pool boling flow
Phase change
Corrugation
Cavities
Geometric investigation

ABSTRACT

This numerical work presents a geometrical investigation of a corrugated isothermal surface placed in a two-dimensional cavity subjected to unsteady, turbulent pool boiling flows. The main purposes are maximizing the heat transfer rate between the isothermal surface and the surrounding water flow, and the volume of vapor generated into the cavity. The geometric investigation followed the constructal design method, being the ratio H_i/L_i (i = 1, 2 or 3) of the corrugations varied for three different numbers of corrugations: N = 1, 2, and 3, keeping constant the corrugations area. The volume of fluid (VOF) and Lee's evaporation-condensation models are used to estimate the volume fractions of water vapor/liquid and interfacial mass transfer. The unsteady Reynolds Averaged Navier Stokes (URANS) continuity, momentum and conservation of energy equations, and volume fraction transport equation, are solved using the finite volume method (FVM) available in software Ansys FLUENT. For closure of turbulence, the k - ε model is adopted. For validation of the model, the heat flux and convection heat transfer coefficient obtained for a pool boiling bared surface case are compared with Rohsenow's correlations, and differences lower than 7.0 % are reached. Results indicated a strong influence of the ratio H_i/L_i and number of corrugations (N) in the heat transfer rate per unit depth (q_s) and dimensionless volume of vapor (V_{dim}) generated into the cavity. The highest intrusion of the corrugations led to the generation of few large and many small scales, benefiting the thermal performance, regardless of the performance indicator employed. The optimal configuration, $N = 3$ and $H_3/L_3 = 2.0$ improved 49 % and 188 % the V_{dim} and q_s compared with the worst corrugated case, showing the importance of the geometry of the corrugation in this problem.

1. Introduction

Boiling flows have been a subject of special interest due to the high heat fluxes involved in this process. Consequently, several thermal equipment such as heat exchangers used in industrial and commercial HVAC (heating, ventilation, and air conditioning), heat pipes, devices for cooling engines in automobiles, aeronautics and marine applications, and cooling of microelectronics packages, are designed to operate under boiling phase change conditions [1–4].

Despite the advantages in terms of heat flux, boiling flows are extremely complex and understanding the influence of certain parameters such as the use of different working fluids, and surface conditions on the quantitative parameters like critical heat flux and heat transfer coefficient is challenging [3,4]. According to Perez-Raya and Kandlikar [2], advancements in techniques such as increasing the density in the nucleation region, inserting fins or re-entrant cavities, and employing porous, hydrophilic and hydrophobic surfaces can further improve the performance in the boiling flows. Recently, Singh and Sharma [4] conducted an important review outlining strategies found in the literature

* Corresponding author.
E-mail address: claudia.naldi2@unibo.it (C. Naldi).

https://doi.org/10.1016/j.ijheatmasstransfer.2024.126334
Received 13 May 2024; Received in revised form 19 September 2024; Accepted 14 October 2024
Available online 20 October 2024

Nomenclature

A_{cav}	Area of the cavity, m^2
A_{cor}	Area of the corrugations, m^2
A_S	Area of heat exchange of the lower surface of the cavity, m^2
Bo_H	Bond number, $g(\rho_l - \rho_v)H^2/\sigma$
C_p	Specific heat, $J{\cdot}kg^{-1}{\cdot}K^{-1}$
F_v	Force per unit volume caused by surface tension, $N{\cdot}m^{-3}$
g	Acceleration of the gravitational field, $m{\cdot}s^{-2}$
Gr_H	Grashof number, $\beta g(T_S - T_\infty)H^3/\upsilon^2$
H	Cavity height, m
h	Convection heat transfer coefficient, $W{\cdot}m^{-2}{\cdot}K^{-1}$
h_{lv}	Latent heat of vaporization, $kJ{\cdot}kg^{-1}$
Ja	Jakob number, $C_P(T_S - T_\infty)/h_{lv}$
k	Turbulent kinetic energy, $m^2{\cdot}s^{-2}$
L	Cavity length, m
N	Number of corrugations, -
p	Pressure, Pa
q_s	Heat transfer rate per unit depth, $W{\cdot}m^{-1}$
T	Temperature, K
T_S	Temperature of the bottom surface, K
T_{sat}	Temperature of saturation of the fluid, K
t	Time, s
u	Velocity in the x-direction, $m{\cdot}s^{-1}$
v	Velocity in the y-direction, $m{\cdot}s^{-1}$
V_{dim}	Dimensionless volume of vapor generated in the cavity, -
V_v	Volume of vapor generated in the cavity, m^3
V_{res}	Volume of the cavity, m^3
Pr	Prandtl number, $\mu C_p/k$
$q"$	Heat flux, $W{\cdot}m^{-2}$
S_m	Mass source representing the mass transfer rate between phases, $kg{\cdot}m^{-3}{\cdot}s^{-1}$
u^*	Friction velocity ($(\tau/\rho)^{1/2}$), $m{\cdot}s^{-1}$
x	Spatial coordinate in free stream direction, m
y	Spatial coordinate in the normal direction to free stream, m
y^+	Dimensionless wall distance in the boundary layer ($y^+ = yu^*/\upsilon$)

Greek symbols

α	Volume fraction of phase, -
β	Thermal expansion coefficient, K^{-1}
ε	Dissipation rate of turbulent kinetic energy, $m^2{\cdot}s^{-3}$
λ	Thermal conductivity, $W{\cdot}m^{-1}{\cdot}K^{-1}$
λ_t	Turbulent thermal conductivity, $W{\cdot}m^{-1}{\cdot}K^{-1}$
μ	Dynamic viscosity, $kg{\cdot}m^{-1}{\cdot}s^{-1}$
υ	Kinematic viscosity, $m^2{\cdot}s^{-1}$
φ	Fraction area of the corrugations, A_{cor}/A_{cav}
ρ	Density, $kg{\cdot}m^{-3}$
σ	Surface tension, $N{\cdot}m^{-1}$
μ_T	Turbulent viscosity, $kg{\cdot}m^{-1}{\cdot}s^{-1}$

Subscripts

m	Once maximized or minimized
mm	Twice maximized or minimized
o	Once optimized
oo	Twice optimized
l	Liquid phase
v	Vapor phase
i	Spatial coordinate or number of corrugations in the problem
1	One corrugation
2	Two corrugations
3	Three corrugations

Superscripts

–	Time-averaged variables

to modify heating surfaces to enhance the heat exchange in pool boiling flows. Various strategies were discussed for designing heating surfaces using nanomatxerial deposition considering different materials [5–8], and incorporating nano and microstructures (micro fins, microgrooves) in the heating surface [9–11]. Moreover, the study indicated recommendations regarding the influence of modified surfaces on parameters such as wettability, nucleation sites, critical heat flux and heat transfer coefficients in pool boiling flows.

Numerical investigations have also been developed seeking to improve the comprehension of the pool and channel boiling flows. Chen et al. [12] performed a comprehensive review showing the advantages, disadvantages, and main applications of three different numerical modeling techniques: microscopic molecular dynamics simulation, mesoscopic lattice Boltzmann, and macroscopic computational fluid dynamics (CFD), the latter used in the present work. According to the authors, the CFD method allows the prediction of the flow field at the fluid/vapor interface and microscopic microlayer surface during boiling, being interesting for the investigation of engineering applications.

First numerical studies were devoted to understanding the different numerical techniques used to simulate the physical problem, seeking to reproduce qualitatively the flow patterns and attend to quantitative aspects such as the conservation of mass and energy, partial pressure, properly tracking the fluid/vapor interface, estimate tension surface and phase transition among different phases [13–15]. For example, Tomar et al. [15] presented an approach based on the coupled level-set and volume of fluid (CLSVOF) method to simulate the growth of bubbles in a two-dimensional pool boiling flow. Two working fluids (water and R134) were simulated for different excesses of temperature. Numerical results predicted the dynamic of vapor bubble, from generation to detachment from the heated surface as a function of the excess of temperature. As time advanced, numerical studies were performed to obtain recommendations about the influence of different configurations on the physical behavior of pool boiling flows. For instance, Zhao et al. [16] numerically investigated the effect of a modified surface, using a combination of microstructures and wetting properties, on the variation of the vapor bubble behavior, fluid dynamic and thermal fields, temperature of solid-liquid interface, and heat transfer coefficient. Later, Singh and Premachandran [17] performed numerical simulations seeking to understand the behavior of the liquid-vapor interface, instability in this region and heat transfer in a wavy wall for saturated horizontal film boiling. Among the author's observations, results indicated that the wave surface influenced the interface liquid/vapor for heater wavelengths larger than the critical Rayleigh-Taylor wavelength. Moreover, the influence of wavy configuration on the film boiling heat transfer was dissimilar to that noticed for single-phase flows.

Recently, Thamil and Premachandran [18] performed a numerical investigation of a saturated pool boiling water flow inserting two inline cylinders into the cavity domain. The authors investigated the influence of different liquid Reynolds numbers (Re_D), different spacing between the two cylinders, and superheat on heat transfer rates. Authors noticed that, for lower spacing between the cylinders, a vapor column is generated in the space between the cylinders for lower spacing magnitudes. This behavior becomes unstable with the increase of the flow rate.

The present work investigates the influence of the height/length ratio for one, two and three symmetrical rectangular corrugations over the volume of water vapor generated into the cavity and the heat transfer rate in the light of constructal design method [19–22]. All cases

FIGURES

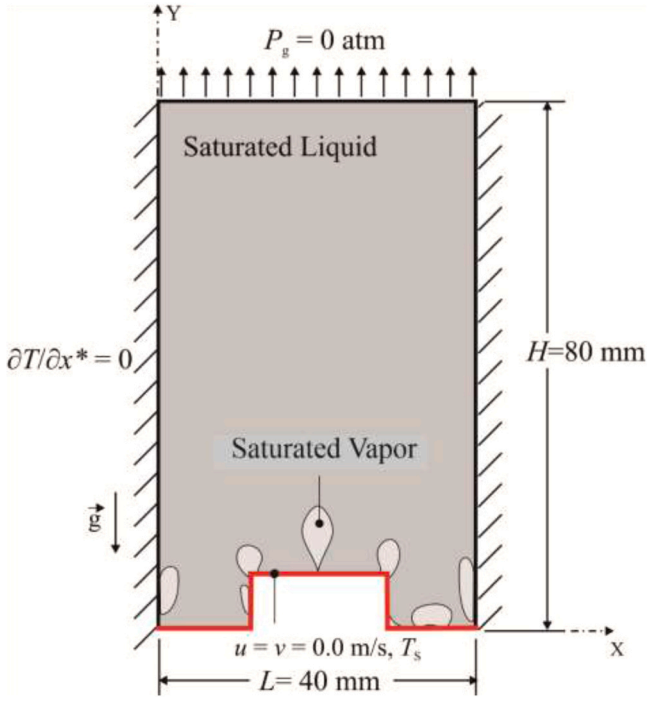

Fig. 1. Computational domain of the cavity with one rectangular corrugation and imposed boundary conditions.

considered a turbulent and two-phase water/vapor flow using Ansys Fluent, version 14.5. Previous applications of constructal design for the geometrical study of intruded fins or blocks in lid-driven cavities [23, 24] or fins of phase change material (PCM) intruded in cavities [25] have been investigated.

The innovation of this work lies in combining computational modeling with the analysis of how geometry influences bubble dynamics and heat transfer efficiency in pool boiling. The main contribution is the application of the constructal design method to investigate the influence of the height-to-length ratio of corrugated surfaces on vapor generation and heat transfer rate during pool boiling. While the constructal design has been previously explored for surfaces with added fins or blocks in cavities and phase change materials (PCM), the study of isothermal corrugated surfaces in cavities for pool boiling flows using this method, to the best of the author's knowledge, has been limited in the literature. This approach offers new perspectives on the design of corrugated surfaces in cavities and significantly advances knowledge in the field of boiling heat transfer.

2. Mathematical modeling

In the present study it is considered a pool boiling flow in cavities with inferior bared and corrugated surfaces. At the beginning of the process, water is completely in a liquid-saturate state, and it is heated by the inferior surface leading the water to boil. It is assumed the domain is two-dimensional, the flow is transient, incompressible and turbulent, and the gravitational field is in only one direction (-y) of the domain. Firstly, it is presented the problem description and how the geometrical investigation is performed with constructal design. In a second moment, it is presented the mathematical modeling of the physical problem applied for all studied configurations.

2.1. Problem description and geometric investigation

The computational domain is a rectangular fluid region, as illustrated in Fig. 1, with dimensions $H = 80$ mm and $L = 40$ mm. The length of the cavity has the same dimension investigated in the work of Sun et al. [26]. Some preliminary tests have also been performed trying to identify the length and height that did not influence the time-averaged q'' and h for validation purposes, and $L = 40$ mm and $H = 80$ mm were the minimal length and height that did not influence the variables for a bared cavity. The fluid is heated by the inferior solid surface, made of polished copper material, and maintained at a constant temperature (T_s) with a magnitude higher than the liquid saturation temperature ($T_{sat} = 373.15$ K for absolute pressure of $p_{abs} = 101.325$ kPa). It is adopted here $T_s = T_{sat} + 18$ K. The lateral surfaces have non-slip and impermeability boundary conditions, i.e., velocities in x and y-directions are null ($u = v = 0$ m/s). Concerning the thermal boundary conditions, the lateral surfaces are modeled as thermally insulated, i.e., $\partial T/\partial x = 0$. The lateral walls are insulated to force the fluid flow to exchange heat only with the inferior surface. In the top region, a null pressure gauge ($p_g = 0$ Pa) and local thermal parabolic condition are assumed. This boundary condition is also similar to that used by Sun et al. [26] and it is employed to avoid the vapor condensation, preventing any influence of the condensation in the boiling process into the cavity. For the initial condition, $t = 0$ s, it is assumed the water is completely in a liquid state and at T_{sat}, i.e., a state in which most of the liquid slightly exceeds the saturation temperature.

Table 1
Data of thermophysical properties and parameters used in the present simulations.

Variable/Phase	Liquid	Vapor
Density (kg·m^{-3})	$\rho_l = 957.9$	$\rho_v = 0.5956$
Dynamic viscosity (N·s·m^{-2})	$\mu_l = 2.79 \times 10^{-8}$	$\mu_v = 1.34 \times 10^{-5}$
Specific heat (kJ·kg^{-1}·K^{-1})	$C_{p,l} = 4.217$	$C_{p,v} = f(T)$
Thermal conductivity (W·m^{-1}·K^{-1})	$\lambda_l = 0.6$	$\lambda_v = 0.0261$
Surface tension (N·m^{-1})	58.9×10^{-3}	
Jakob number (Ja)	$Ja = 0.031$	
Bond number (Bo_H)	$Bo_H = 1020.43$	
Grashof number (Gr_H)	$Gr_H = 2.2 \times 10^{16}$	

The thermophysical properties adopted for water and vapor in the present problem as density (ρ), dynamic viscosity (μ), specific heat (C_p), latent heat of vaporization (h_{lv}) and surface tension (σ) are represented in Table 1. The Jakob, Bond and Grashof numbers adopted for all cases studied here are also presented in Table 1. These dimensionless parameters are given by [27]:

$$Ja = \frac{C_P(T_S - T_\infty)}{h_{lv}} \tag{1}$$

$$Bo_H = \frac{g(\rho_l - \rho_v)H^2}{\sigma} \tag{2}$$

$$Gr_H = \frac{\beta g(T_S - T_\infty)H^3}{\nu^2} \tag{3}$$

where β is the thermal expansion coefficient of the water at 100 °C (K^{-1}), and the subscripts l and v represent the liquid and vapor phases, respectively.

Note that it is considered the thermophysical properties of the liquid phase as constant because, for the temperature range evaluated, the variation of these properties is less significant compared to the vapor phase [28].

The specific heat of the vapor phase (in J·kg^{-1}·K^{-1}) is modeled using a partial polynomial function of temperature for a specified range of temperature (300 K $\leq T \leq$ 1000 K) as follows [28]:

$$C_{p,v}(T) = 1563.077 + 1.603755\ T - 2.932784 \times 10^{-3}T^2 + 3.216101 \times 10^{-6}T^3 - 1.156027 \times 10^{-9}T^4 \tag{4}$$

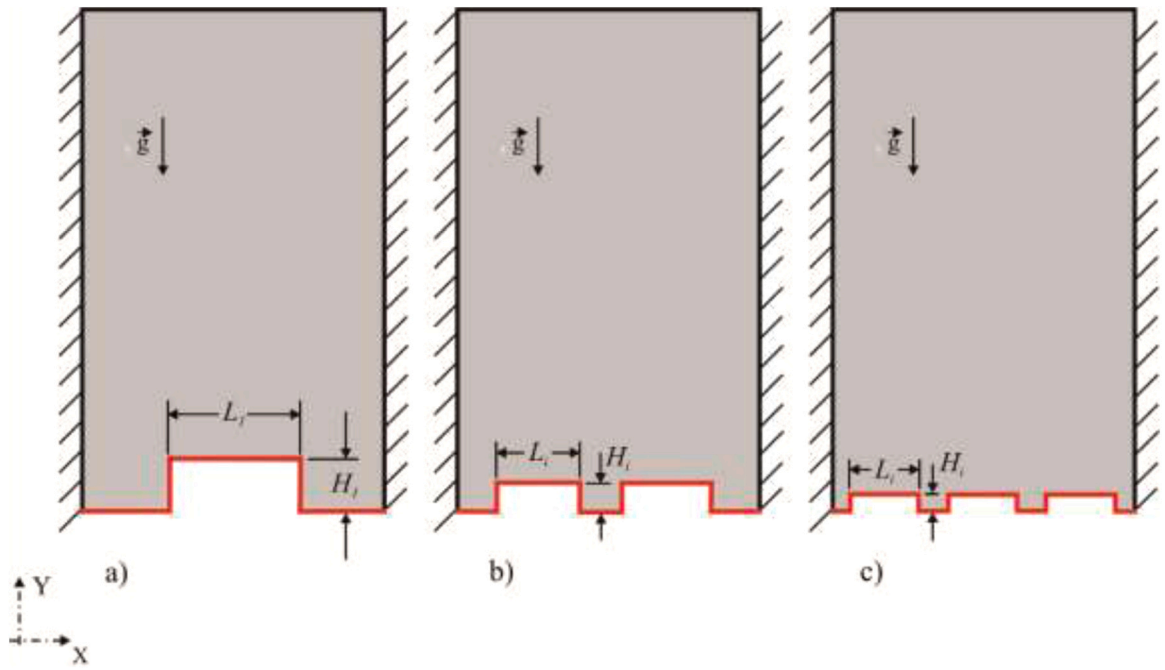

Fig. 2. Schematic illustration of the cavity domain with different numbers of corrugations in the inferior wall: a) $N = 1$, b) $N = 2$, c) $N = 3$.

Concerning the geometrical investigation, three different cases with different quantities of rectangular corrugations mounted at the base of the reservoir are studied in addition to the bared surface, which is used for verification/validation of the computational method. Each case presented in Fig. 2 has a defined number of corrugations, N. The first with one corrugation placed in the center of the inferior surface, Fig. 2 (a), the second with two corrugations, Fig. 2(b), and the third one with three corrugations, Fig. 2(c). The geometrical investigation is realized using the constructal design method [19–22], following the steps described in the flowchart of Fig. 3.

The problem is subjected to two constraints, the total area of the cavity (A_{cav}) and the area occupied by the corrugations (A_{cor}), as given by:

$$A_{cav} = HL \tag{5}$$

$$A_{cor} = N{\cdot}(H_i L_i) \tag{6}$$

where H_i and L_i are the height and length of the corrugations (m), the subscript i is an indication of the case investigated: (1) one corrugation, (2) two corrugations, and (3) three corrugations. The area of the corrugation can also be represented in dimensionless form by:

$$\varphi = \frac{A_{cor}}{A_{cav}} \tag{7}$$

The magnitude of $\varphi = 0.03125$ is adopted for all configurations, regardless of the number of corrugations investigated. It is worth mentioning that the total heat exchange area (A_s) is the total bottom surface of the reservoir, as given by:

$$A_S = L + 2H_i N \tag{8}$$

For this work, the performance indicators adopted are the dimensionless vapor volume, V_{dim}, and the heat transfer rate between the isothermal surface and the surrounding cavity flow, q_s, as written by:

$$V_{dim} = \frac{V_v}{V_{cav}} \tag{9}$$

$$q_s = hA_S(T_S - T_{sat}) \tag{10}$$

where V_v is the volume of vapor generated along the time interval of each simulation (m^3), V_{cav} is the volume of the cavity (m^3). For the two-dimensional domain, it is considered the areas of the generated vapor and the reservoir.

The geometric investigation performed here consists of two steps, as depicted in Fig. 4. In the first step, the degree of freedom H_1/L_1 is varied in the range $0.25 \leq H_1/L_1 \leq 2.0$ for the configuration with $N = 1$. The highest magnitudes of V_{dim} and q_s are the once maximized dimensionless generated vapor $(V_{dim})_m$ and heat transfer rate $(q_s)_m$. The corresponding height/length ratio is the once optimized ratio H_1/L_1, $(H_1/L_1)_o$. In the second step, the same procedure adopted for $N = 1$ is repeated for the other cases ($N = 2$ and 3), obtaining the magnitudes of $(V_{dim})_m$ and $(q_s)_m$ and the corresponding optimal configurations $(H_2/L_2)_o$ and $(H_3/L_3)_o$, where subscripts 2 and 3 refer to $N = 2$ and 3, respectively. For $N = 2$ and 3, it is adopted a symmetrical variation for the different corrugations mounted in the lower surface of the cavity. The highest magnitudes of V_{dim} and q_s among all studied cases are the twice maximized dimensionless generated vapor $(V_{dim})_{mm}$ and heat transfer rate $(q_s)_{mm}$, and the corresponding optimal configurations are $(H_i/L_i)_{oo}$ and N_o. Despite the notation used here, the analysis is restricted to a geometrical investigation, seeking to obtain the trend of the corrugations design in the pool boiling cavity problem. An optimization study is not performed here, since an optimization method is not associated with the geometrical investigation. Moreover, the number of investigated cases is limited due to the physical complexity and computational effort required for the problem. A total of thirteen simulations were performed, twelve varying the ratio H_i/L_i in the range $0.25 \leq H_i/L_i \leq 2.0$, and one more simulation with bared surface, which is simulated for problem validation and to compare with the cases with corrugations.

2.2. Governing equations of the boiling flow

The volume of fluid (VOF) method is used to tackle the two phases (water liquid and vapor). The unsteady-RANS (URANS) time-averaged conservation equation of mass, the momentum equation and energy equation for the transient solution of mixture liquid/vapor of water can be given by [27,29]:

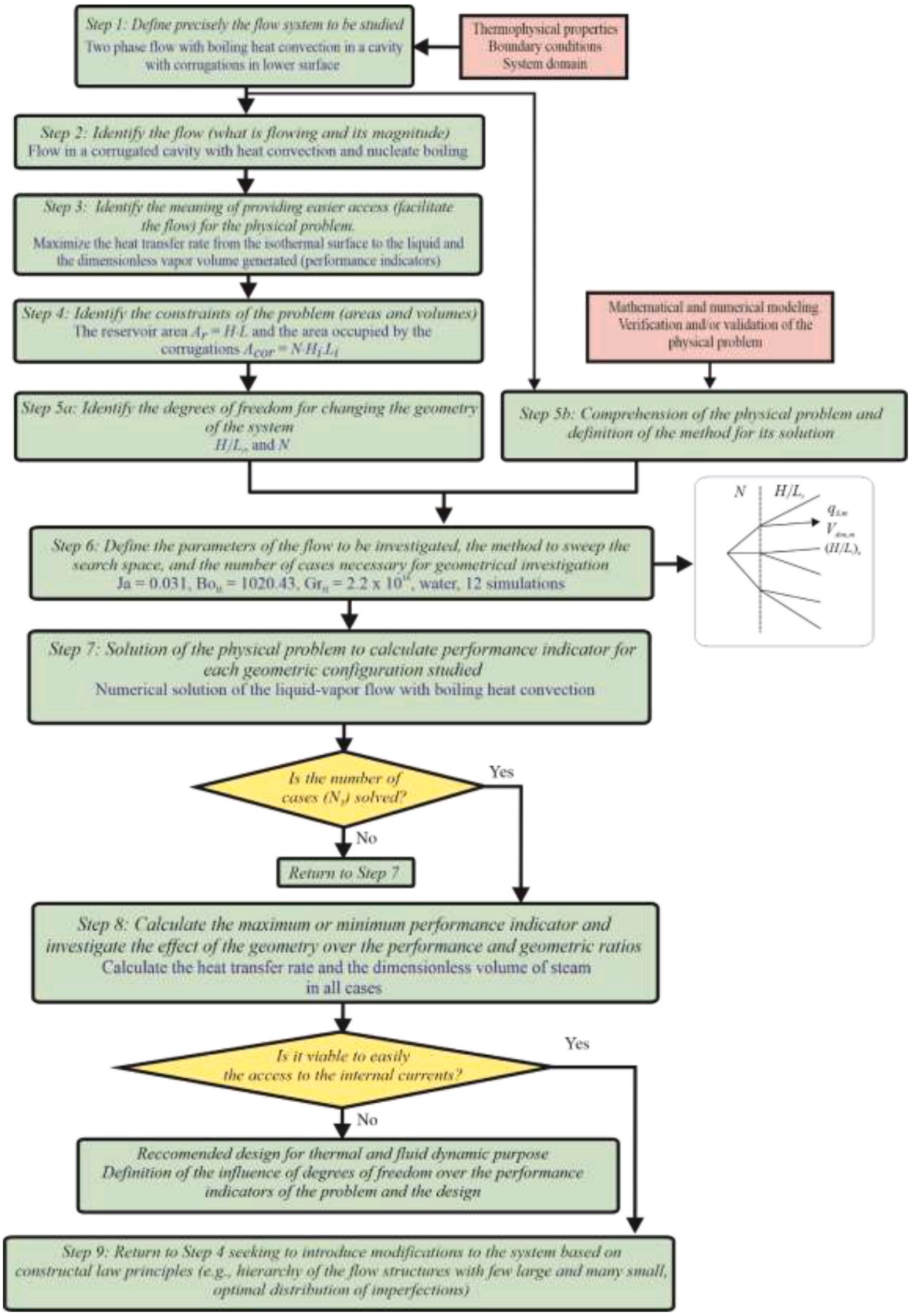

Fig. 3. Flowchart of the geometrical investigation employed in the present problem with Constructal Design.

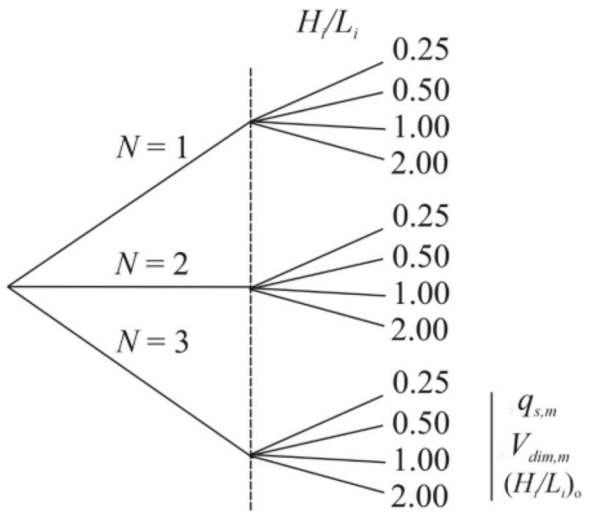

Fig. 4. Scheme of simulations defined with Constructal Design for geometrical investigation with varied number of corrugations (*N*).

$$\frac{\partial \rho}{\partial t} + \frac{\partial}{\partial x_j}\left(\rho \bar{v}_j\right) = S_m \tag{11}$$

$$\frac{\partial \rho \bar{v}_i}{\partial t} + \bar{v}_j \frac{\partial}{\partial x_j}\left(\rho \bar{v}_i\right) = -\frac{\partial \bar{p}}{\partial x_i}\delta_{ij} + \left(\mu + \mu_t\right)\frac{\partial}{\partial x_j}\left(\frac{\partial \bar{v}_i}{\partial x_j} + \frac{\partial \bar{v}_j}{\partial x_i}\right) + \rho g_i + F_{v,i} \tag{12}$$

$$\frac{\partial \rho \bar{E}}{\partial t} + \bar{v}_j \frac{\partial}{\partial x_j}\left(\rho \bar{E}\right) = \left(\lambda + \lambda_t\right)\frac{\partial^2 \bar{T}}{\partial x_j^2} + S_h \tag{13}$$

where ρ is the density of the mixture ($kg{\cdot}m^{-3}$), $\bar{v}$ is the time-averaged velocity ($m{\cdot}s^{-1}$), g is gravitational acceleration ($m{\cdot}s^{-2}$), μ is the dynamic viscosity of the mixture ($kg{\cdot}m^{-1}{\cdot}s^{-1}$); μ_t is the turbulent dynamic viscosity ($kg{\cdot}m^{-1}{\cdot}s^{-1}$), t is the time (s), $\bar{T}$ is the time-averaged temperature (K), λ is the thermal conductivity of the mixture ($W{\cdot}m^{-1}{\cdot}K^{-1}$) and λ_t the turbulent thermal conductivity ($W{\cdot}m^{-1}{\cdot}K^{-1}$), S_m is the mass source representing the mass transfer rate ($kg{\cdot}m^{-3}{\cdot}s^{-1}$), $F_{v,i}$ represents the force per unit volume caused by surface tension ($N{\cdot}m^{-3}$) and S_h is the heat generation per unit volume ($W{\cdot}m^{-3}$). In addition, the suffix i and j refers to the Cartesian components and the upper horizontal line, overline, is the time-averaged operator.

For closure of turbulent flows, the classical model k - ε based on the Unsteady Reynolds Averaged Navier Stokes (URANS) approach is used. In this modeling, the turbulent viscosity and conductivity are given, respectively, by [29,30]:

$$\mu_t = \frac{C_\mu \rho k}{\varepsilon} \tag{14}$$

$$\lambda_t = \frac{C_p \mu_t}{Pr_t} \tag{15}$$

The turbulent kinetic energy (k) and the dissipation rate of turbulent kinetic energy (ε) are obtained with two additional transport equations, given by:

$$\frac{\partial k}{\partial t} + \bar{v}_j \frac{\partial k}{\partial x_j} = \tau_{ij}\frac{\partial \bar{v}_i}{\partial x_j} + \frac{\partial}{\partial x_j}\left[\left(\upsilon + \frac{\upsilon_t}{\sigma_k}\right)\frac{\partial k}{\partial x_j}\right] - \varepsilon \tag{16}$$

$$\frac{\partial \varepsilon}{\partial t} + \bar{v}_j \frac{\partial \varepsilon}{\partial x_j} = \frac{\partial}{\partial x_j}\left[\left(\upsilon + \frac{\upsilon_t}{\sigma_\varepsilon}\right)\frac{\partial \varepsilon}{\partial x_j}\right] + C_{\varepsilon 1}\frac{\varepsilon}{k}\tau_{ij}\frac{\partial \bar{v}_i}{\partial x_j} - C_{\varepsilon 2}\frac{\varepsilon^2}{k} \tag{17}$$

where $C_\mu = 0.09$, $Pr_t = 1.0$, $C_{\varepsilon 1} = 1.44$, $C_{\varepsilon 2} = 1.92$, $\sigma_k = 1.0$, and $\sigma_\varepsilon = 1.3$ are ad hoc constants of the closure model. These are standard coefficients used by the Fluent software, already employed by other authors in studies involving phase change [31–33]. According to Zhang et al. [33], for phase change boiling flows, the $k - \varepsilon$ closure model led to a better agreement than $k - \omega$ with experimental results for predicting void fraction and temperatures. Considering it is also less time-consuming in comparison with other URANS modeling as $k - \omega$, and Reynolds Stress Tensor, the $k - \varepsilon$ is selected to be used in the present study.

Here, the liquid/vapor interface tracking process is performed using the VOF method [34]. In this model, the transient mass, momentum and energy equations are solved for the mixture and the volume fraction for each phase is estimated by one additional transport equation.

According to Hirt and Nichols [34], the volume fraction of all phases adds up to the unit in the computational cell. Depending on its value, the specific properties and variables of each problem are assigned to each control volume within the domain. The sum of the water and vapor volume fraction is given by:

$$\alpha_l + \alpha_v = 1 \tag{18}$$

For a condition where the cell is empty of liquid water, the $\alpha_l = 0.0$ and $\alpha_v = 1.0$. Conversely, for the cell empty of vapor, the $\alpha_l = 1.0$ and $\alpha_v = 0.0$. In the interface tracking process, a transport equation is solved for the volume fraction in each phase. The volume fraction of liquid water (α_l) in any position and time of the domain is defined by the following transport equation [34]:

$$\frac{1}{\rho_l}\left[\frac{\partial}{\partial t}\left(\alpha_l \rho_l\right) + \nabla\cdot\left(\vec{v}_l \alpha_l \rho_l\right) = S_{\alpha l} + \sum_{v=1}^{n}\left(\dot{m}_{vl} - \dot{m}_{lv}\right)\right] \tag{19}$$

where $\dot{m}_{vl}$ is the mass transfer from phase v to phase l and $\dot{m}_{lv}$ mass transfer from phase l to phase v ($kg{\cdot}m^{-3}{\cdot}s^{-1}$). The $\dot{m}_{vl}$ corresponds to the condensation process and the $\dot{m}_{lv}$ to the boiling process.

To quantify the mass transfer through the interfaces, the model proposed by Lee [35] was used. In this model, the process of transferring liquid-vapor mass is governed by the following equations and temperature conditions:

$T_l > T_{sat}$ – evaporation process:

$$\dot{m}_{lv} = coef{\cdot}\alpha_l \rho_l \frac{\left(T_l - T_{sat}\right)}{T_{sat}} \tag{20}$$

$T_v < T_{sat}$ – condensation process:

$$\dot{m}_{vl} = coef{\cdot}\alpha_v \rho_v \frac{\left(T_{sat} - T_v\right)}{T_{\text{sat}}} \tag{21}$$

where *coef* is the coefficient interpreted as a relaxation factor of mass transfer in unit of time (1/s). Some empirical values for *coef* were presented by Sun et al. [26], as well as theoretical formulations obtained from Fourier's law that can be used to overcome the limitations found by the use of expressions and empirical coefficients. In the numerical study by Machado and Cabral [36], the results of seven combinations for the coefficients were tested and presented. The authors highlighted the values of 0.1 s^{-1} for evaporation and 1.0 s^{-1} for condensation as the ideal combination for the nucleated boiling problem in a thermosyphon. The recommendation of *coef* = 0.1 s^{-1} for boiling problems is also indicated in the work of Chen et al. [12], being used here.

The mixture thermophysical properties are obtained from the volume fraction and can be written by [37]:

$$\begin{aligned} \rho &= \alpha_v \rho_v + (1 - \alpha_v)\rho_l \\ \mu &= \alpha_v \mu_v + (1 - \alpha_v)\mu_l \end{aligned} \tag{22}$$

In the VOF method, the surface tension is calculated using the Continuum Surface Force (CSF) model proposed by Brackbill et al. [38]. The divergence theorem is used to express the surface force in terms of a volumetric force. This force appears as a source term and is expressed using the following simplified equation for two phases:

$$F_v = \sigma \frac{\rho \eta_l \nabla \alpha_l}{\frac{1}{2}\left(\rho_l + \rho_v\right)} \tag{23}$$

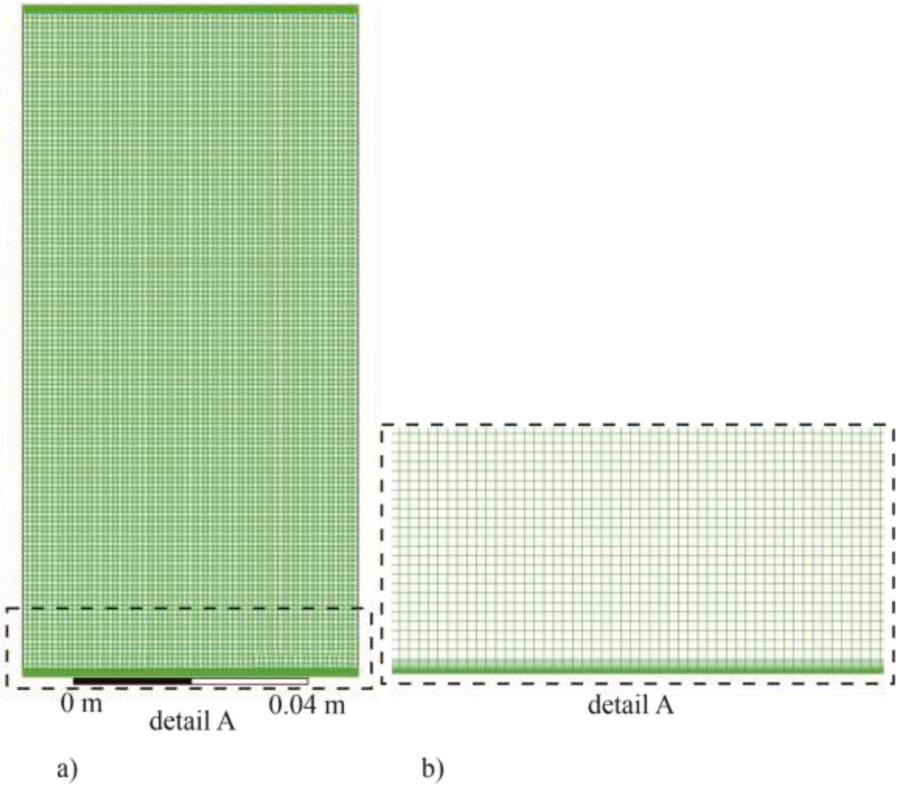

Fig. 5. Grid composed of rectangular surfaces used in the cavity without corrugation: a) whole domain, b) detail of the stretched mesh used in the near wall region.

where η_l is the surface curvature of the interface, calculated by local gradients of the volume fraction from the normal phase to the surface, given by the following relationships:

$$n = \nabla\alpha_v$$
$$\hat{n} = \frac{n}{|n|} \tag{24}$$
$$k = \nabla\hat{n} = \nabla\cdot\left(\frac{\nabla\alpha_v}{|\nabla\alpha_v|}\right)$$

For all phases, a single energy equation is solved in the estimation of the temperature field, as shown in the following equation for each phase:

$$E = \frac{\sum_{q=1}^{n}\alpha_q\rho_q E_q}{\sum_{q=1}^{n}\alpha_q\rho_q} \tag{25}$$

For the two phases considered, the energy is given by:

$$E = \frac{\alpha_l\rho_l E_l + \alpha_v\rho_v E_v}{\alpha_l\rho_l + \alpha_v\rho_v} \tag{26}$$

where E_l and E_v for each phase is a function of specific heat and temperature. In the work developed by Sun et al. [26] an expression is found for each of these variables, described as follows:

$$E_l = C_{p,l}(T - 298.15)$$
$$E_v = C_{p,v}(T - 298.15) \tag{27}$$

3. Numerical modeling and code validation

For the numerical solution, the conservation equations of mass, momentum and energy, as well as the volume fraction transport equation, are solved with the Finite Volume Method (FVM) that is available in the software Ansys Fluent, version 14.5 [39–41]. The following numerical procedures, available in Ansys Fluent, are adopted in the present simulations:

(i) The second order upwind spatial interpolation scheme is adopted for the momentum and energy equations;
(ii) The geo-reconstruct scheme is used to tackle the reconstruction of the interface liquid/vapor distribution;
(iii) Residuals of 1.0×10^{-6} are used for the mass, momentum and energy equations to achieve the convergence at each time step;
(iv) For the pressure-velocity coupling solution, the SIMPLE algorithm is employed;
(v) The explicit first order scheme for advancing time with interval (Δt) is adopted, based on the Courant number of 0.25, for the volume fraction transport equation;
(vi) In the modeling of turbulence of the regions close to the wall the enhanced treatment ε-equation method (EWT-ε) is used.

It should be noted that the calculated value for y^+ maintained an average of approximately 10, which is recommended for the use of k - ε model with the employment of the law of wall [29]. The dimensionless distance of the turbulent boundary layer is given by [29]:

$$y^+ = \frac{y\sqrt{\tau_w/\rho}}{\nu} = \frac{yu^*}{\nu} \tag{28}$$

where y is the normal distance to the wall (m), τ_w is the surface tension in the wall ($N\bullet m^{-2}$), υ is the kinematic viscosity ($m^2\bullet s^{-1}$), and u^* is the friction velocity ($m\bullet s^{-1}$).

All cavity problems are simulated along the time interval of $t = 1.0$ s. The heat flux in the lower surface is monitored (q") along the time interval 0.5 s $\leq t \leq$ 1.0 s. The volume of vapor generated is monitored along all time interval, but the final instant of time ($t = 1.0$ s) is used to calculate the V_{dim} for each case. For all cases, a constant time-step of $\Delta t = 1.0 \times 10^{-4}$ s is adopted. The simulations were performed in a computer with an Intel Core i7 @ 3.3 GHz processor and 16 GB of RAM. The computational effort for the performed simulations is nearly $t_{proc} = 2.6 \times$

Table 2
Mesh independence study for the case of cavity with inferior bared surface.

Number of volumes	h (W.m^{-2}.K^{-1})	q''(W·m^{-2})	$\left\|\left(q''_j - q''_{j+1}\right)/q''_j\right\|$	Computational effort (h)
7140	23,899.06	430,183	0.136	12.4
15,040	27,166.33	488,994	0.363	30.6
31,680	37,049.60	666,894	0.054	72.2
63,000	35,032.06	630,577	——	251.7

Table 3
Comparison of q'' and h obtained with the present method and the correlation of Rohsenow [42] for $\Delta T_e = 18$ °C.

Variable/Method	Present work	Rohsenow [42]	Deviation (%)
q'' (W·m^{-2})	666,894	714,035	6.60
h (W·m^{-2}·K^{-1})	37,049.6	39,648.4	6.55

10^5 s (72.2 h) for the case with bared surface and around $t_{proc} = 4.3 \times 10^5$ s (119.4 h) for the cases with corrugated surfaces.

It is worth mentioning that, in the present work, it is considered a small domain and the initial condition with the fluid at saturated temperature. These conditions speed up the boiling process, allowing the achievement of the fully developed boiling state for the time interval investigated here.

For the validation of the numerical tool, it is firstly performed the study of grid sensitivity for the case of the cavity with an inferior bared surface. A structured grid with rectangular finite volumes is generated with the software Ansys Design Modeler available in Ansys Workbench – version 14.5. In Fig. 5(a) a general view of the mesh is presented, while in Fig. 5(b) a detailed view of the mesh near the inferior wall, where the mesh is more refined due to the generation of the boiling and steps gradients of velocity and temperature in this region. In this region, a stretched strategy for the mesh is employed using a growth ratio of 1.05 from the minimal volume (near the surface) towards the region less affected by the wall. Near the wall, at least 20 vol layers were used to refine the mesh.

The appropriate mesh is obtained by successive refinements resulting in meshes with different quantities of elements until the criterium $\left|\left(q''_j - q''_{j+1}\right)/q''_j\right| < 1.0 \times 10^{-1}$, where the subscripts "$j$" represents the heat flux obtained with the coarse mesh and "$j+1$" represents the next refined mesh. The heat flux is calculated in the software by the prediction of the dimensional temperature gradient at several points of the inferior surface, and an average of these gradients is taken. Based on this value and on the local volume fraction, the software applies the Fourier's law to the wall to calculate the instantaneous heat flux in the lower surface of the cavity. Table 2 presents the results obtained from the grid independence study for the heat flux (q'') and the magnitudes of h in the inferior surface are also presented. A mesh with nearly 32,000 vol is considered independent in the present investigation, and the refinement characteristics are used for all studied cases. Since the domain is relatively simple, it is possible to keep mesh quality parameters as skewness and orthogonal quality in magnitudes as 0.10 and 0.98, respectively, which is considered excellent in the documentation of Fluent software [41]. The mesh parameters of refinement and mesh quality are used for the corrugated surfaces, leading to slight increase in the number of rectangular volumes generated in the domain.

To validate the present model, the results of the heat flux (q'') and convection heat transfer coefficient (h) in the lower surface of the cavity are compared with experimental correlations of Rohsenow [42] for the same thermal conditions, which are respectively given by:

$$q'' = \mu_l h_{lv} \left(\frac{g(\rho_l - \rho_v)}{\sigma}\right)^{1/2} \left(\frac{C_{p,l}(T_S - T_{sat})}{C_{s,f} h_{lv} Pr_l^n}\right)^3 \quad (29)$$

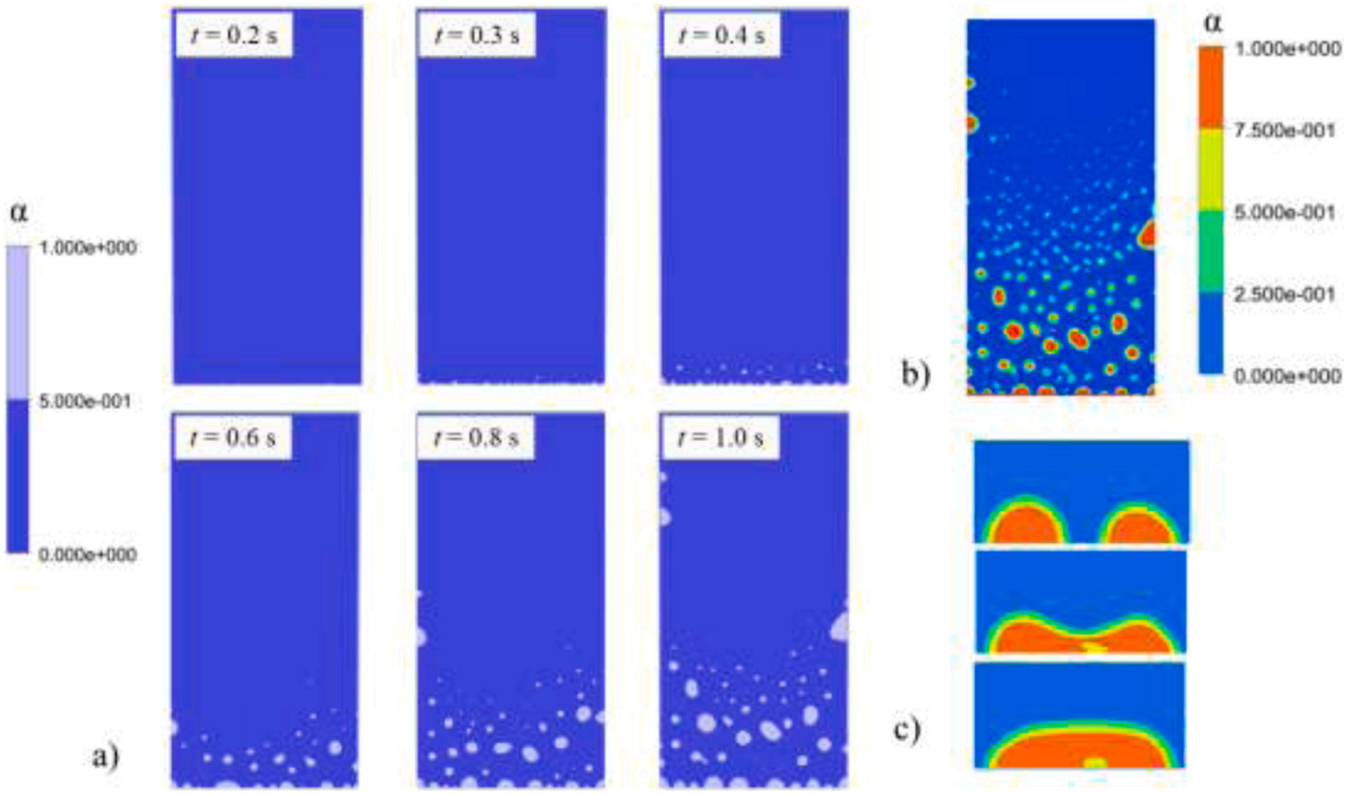

Fig. 6. Volume fraction of vapor (α) in the cavity without corrugation for $\Delta T_e = 18$ °C and different instants of time: a) different time steps, b) $t = 1.0$ s (more scales of volume fraction), c) detailed view of the initial steps of vapor generation.

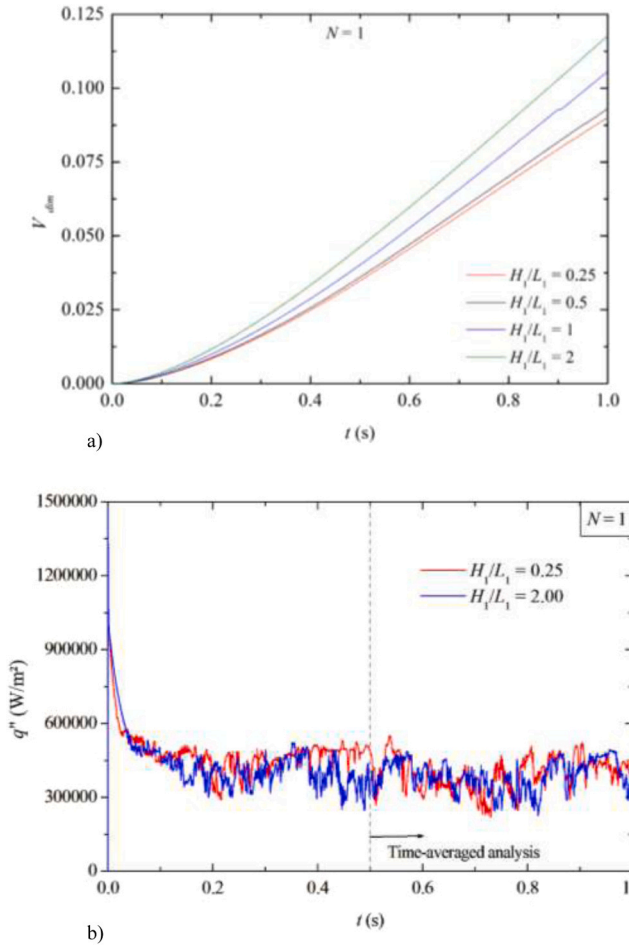

Fig. 7. Instantaneous magnitudes for the configuration with one corrugation (N = 1) and different magnitudes of H_1/L_1: a) dimensionless volume of vapor (V_{dim}), b) heat flux in the lower surface (q'').

$$h = \mu_l h_{lv}\left(\frac{\sigma}{g(\rho_l-\rho_v)}\right)^{-1/2}\left(\frac{C_{p,l}}{C_{s,f}h_{lv}Pr_l^n}\right)^3 (T_S - T_{sat})^2 \quad (30)$$

where $C_{s,f} = 0.0128$ and $n = 1.0$ for the polished copper surface of the cavity with the water as the working fluid.

Table 3 shows the results for q'' and h obtained with the present method and those predicted with the Rohsenow correlation [42] for an excess of temperature $\Delta T_e = T_S - T_{sat} = 18$ °C, which is used in the cases of geometrical investigation. As can be observed, differences in the range of 6.6 % were obtained, which can be acceptable considering the complexity of the physical problem.

In the performed simulation, the physical mechanism of pool boiling flow is reproduced. To illustrate this behavior, Fig. 6(a) shows the volume fraction for different instants of time ($t = 0.2$ s, 0.3 s, 0.4 s, 0.6 s, 0.8 s, and 1.0 s). Fig. 6(b) shows the volume fraction at $t = 1.0$ s for more scales of volume fraction. The simulation time is enough to capture some patterns of the pool boiling as the initial nucleation of the bubbles, coalescence, detachment of vapor bubbles, and the stabilization of turbulent boiling flow. The first points of nucleation of vapor bubbles arise around $t = 0.2$ s and 0.4 s. Later, the first coalescence among the vapor bubbles happened generating larger scales of the bubbles followed by detachment and displacement of the vapor bubbles in bubbly and slug regimes toward the superior part of the cavity. Fig. 6(c) illustrates in detail the initial patterns of the vapor generation, from the initial bubbles up to the formation of a superheated steam bag. This behavior is quite similar to that observed experimentally by Mukherjee and Dhir [13], demonstrating that the present computational method is able to represent qualitatively the vapor generation in pool boiling flows. The bubbles' detachment and their rise in the pool boiling were also compared with numerical simulations of Son and Dhir [43] showing resembling patterns.

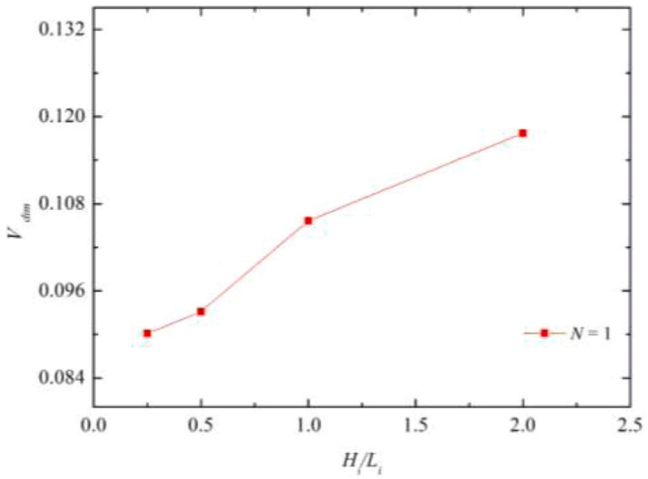

Fig. 8. Effect of the ratio H_i/L_i ($i = 1$) over the dimensionless vapor volume generated in the cavity (V_{dim}) for a cavity with one rectangular corrugation (N = 1).

4. Results and discussion

Firstly, it is investigated the transient behavior of dimensionless volume of vapor generated in the cavity (V_{dim}) for different ratios of H_1/L_1, and spatial averaged heat flux (q'') in the lower surface of the cavity for extreme ratios of H_1/L_1, when $N = 1$, Fig. 7(a) and 7(b), respectively. In Fig. 7(a), it is noticed a small ratio of increase of vapor generated at the beginning of the process, $0.0\ s \leq t \leq 0.2$ s, followed by an increase in the variation of V_{dim} with time, regardless of the ratio of H_1/L_1 applied to the corrugation in the lower surface. Despite of similar trend, the augmentation of the ratio H_1/L_1 led to an increase of the magnitude of the V_{dim} for the different periods analyzed. The differences are more prominent when the corrugations have the highest intrusion into the cavity, $H_1/L_1 = 1.0$ and 2.0. Moreover, the change of the ratio of V_{dim} with time is hasted with the increase of the ratio H_1/L_1, which is an indication that the coalescence of initial bubbles, generation of higher structures and detachment of bubbles in bubbly, and slug regimes is intensified with the insertion of the corrugation and increase of its ratio H_1/L_1. Fig. 7(b) shows the spatial averaged q'' as function of time for $H_1/L_1 = 0.25$ and 2.00, and $N = 1$. It is possible to notice a step decrease in q'' in the interval $0.0\ s \leq t \leq 0.2$ s followed by a stabilization of the mean magnitudes of heat flux, especially for $t \geq 0.5$ s, regardless of the H_1/L_1 ratio. Results also indicated that the mean q'' does not suffer strong variation for the different ratios of H_1/L_1, q'' obtained for $H_1/L_1 = 0.25$ is nearly 7.0 % superior than the ratio $H_1/L_1 = 2.0$. This behavior benefits the highest ratios of H_1/L_1 since the heat exchange area for $H_1/L_1 = 2.0$ is 36.5 % superior than that reached with the lowest ratio $H_1/L_1 = 0.25$, compensating the difference of heat flux and increasing the heat transfer rate when the corrugation has the highest intrusion in the cavity.

Fig. 8 shows the effect of the ratio H_1/L_1 over V_{dim} obtained at $t = 1.0$ s, the last instant of time analyzed for all cases. For the lowest ratios of $H_1/L_1 = 0.25$ and 0.5, the performance in terms of maximizing the volume of vapor generated is quite similar. After this point, there is an increase in the range $0.5 \leq H_1/L_1 \leq 1.0$ followed by another growth, with a smaller ratio, in the range $1.0 \leq H_1/L_1 \leq 2.0$. The case with $H_1/L_1 = 2.0$ led to a magnitude of V_{dim} 30.6 % superior to the case with $H_1/L_1 = 0.25$ (with the lowest intrusion). Fig. 9 illustrates the volume fraction of vapor generated in the cavity for different ratios H_1/L_1: $H_1/L_1 = 0.25$ (Fig. 9(a)), $H_1/L_1 = 0.5$ (Fig. 9(b)), $H_1/L_1 = 1.0$ (Fig. 9(c)), $H_1/L_1 = 2.0$

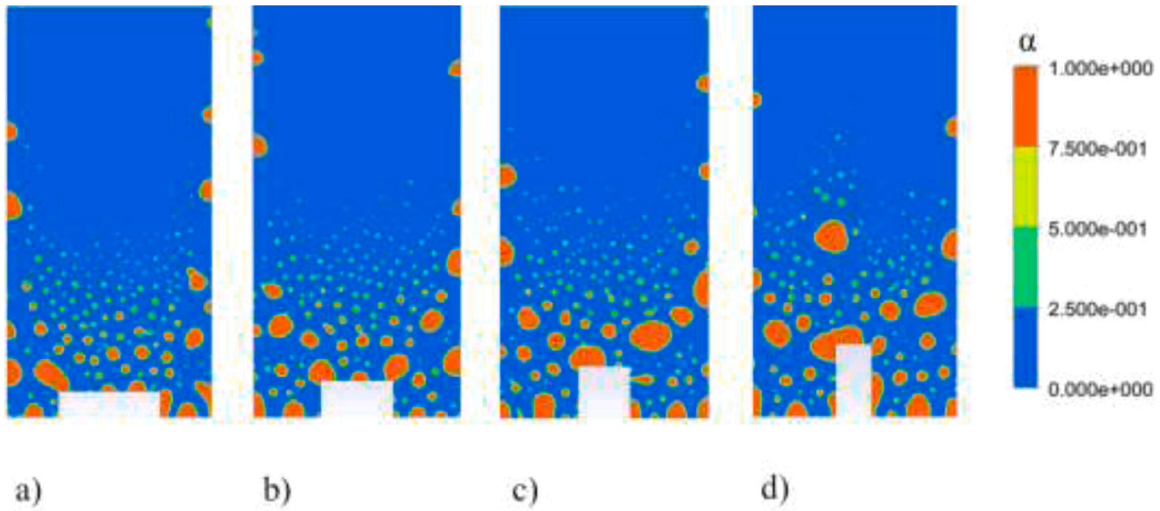

Fig. 9. Volume fraction of vapor generated in the cavity with one corrugation at $t = 1.0$ s for different ratios of H_i/L_i ($i = 1$): a) $H_i/L_i = 0.25$, b) $H_i/L_i = 0.5$, c) $H_i/L_i = 1.0$, d) $H_i/L_i = 2.0$.

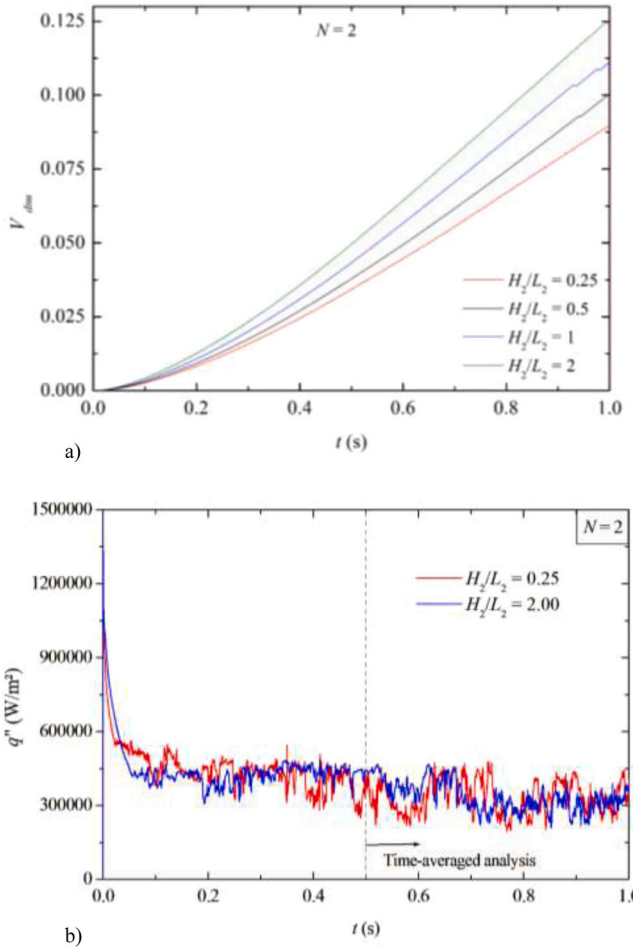

Fig. 10. Instantaneous magnitudes for the configuration with two corrugations ($N = 2$) and different magnitudes of H_i/L_i ($i = 2$): a) dimensionless volume of vapor (V_{dim}), b) heat flux in the lower surface (q'').

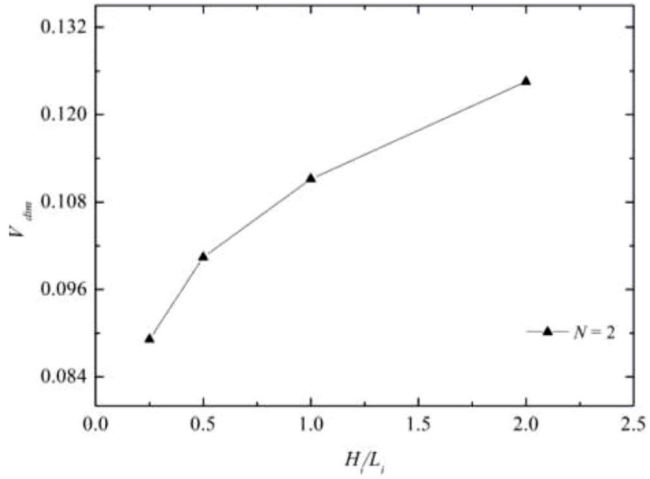

Fig. 11. Effect of the ratio H_i/L_i ($i = 2$) over the dimensionless vapor volume generated in the cavity (V_{dim}) for a cavity with two rectangular corrugations ($N = 2$).

(Fig. 9(d)). It can be noticed that the size of the detached bubbles of vapor in the bubbly regime increases with the augmentation of the ratio H_1/L_1, i.e., the increase of the intrusion of the corrugation intensified the multiplicity of scales of vapor generated in the cavity, intensifying the occurrence of bubbly and slug regimes. This behavior agrees with the constructal law principle that states the flow system structures organize themselves in few large and many small to benefit the whole system. In general, it was verified that the deformations of the bubbles occurred mainly due to the coalescence of the vapor bubbles associated with the natural convection of liquid water flow. It is also noticed that the vapor generated along the gaps interacts with the bubbles generated along the isothermal vertical walls of the corrugation, leading to a more intense interaction between different bubbles. Consequently, the bubbles' detachment towards the upper and lateral regions of the cavity is also intensified. Another interesting aspect is the space between the lateral surfaces of corrugations and the cavity. For the lowest ratios of H_1/L_1, few nucleation sites were found due to the restricted space between the lateral surfaces of corrugation and cavity in comparison with the higher intruded corrugations.

The effect of the insertion of more than one corrugation over V_{dim} and instantaneous q'' are obtained in the first moment keeping $N = 2$. Fig. 10 (a) shows the V_{dim} as a function of time for different ratios of H_2/L_2, while Fig. 10(b) shows the q'' as function of time for extreme magnitudes of H_2/L_2. It is worth noting again that the corrugations are symmetrical in the present investigation, i.e., the ratio H_2/L_2 represents the height/

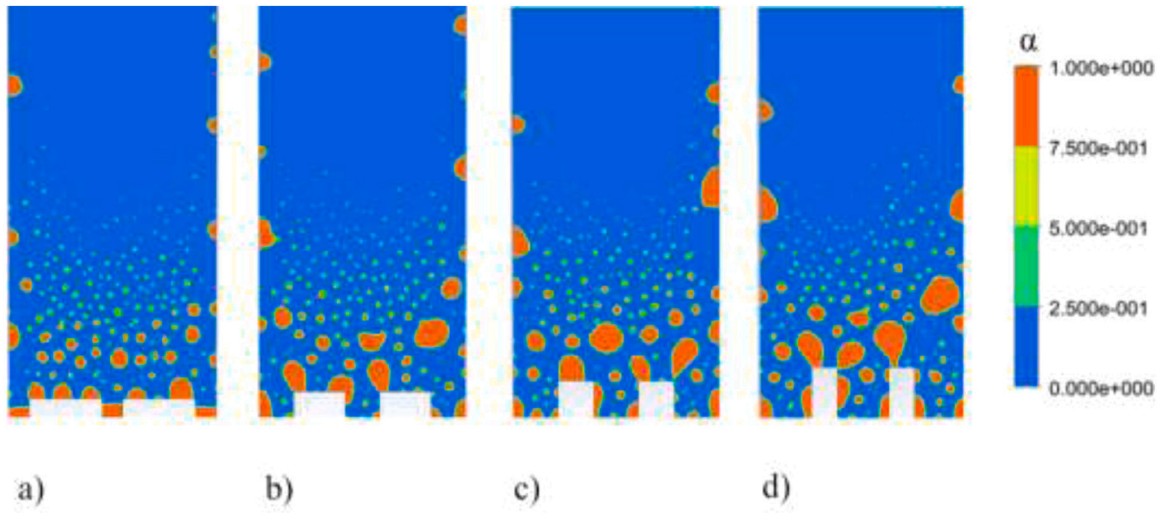

Fig. 12. Volume fraction of vapor generated in the cavity with two corrugations at $t = 1.0$ s for different ratios of H_i/L_i ($i = 2$): a) $H_i/L_i = 0.25$, b) $H_i/L_i = 0.5$, c) $H_i/L_i = 1.0$, d) $H_i/L_i = 2.0$.

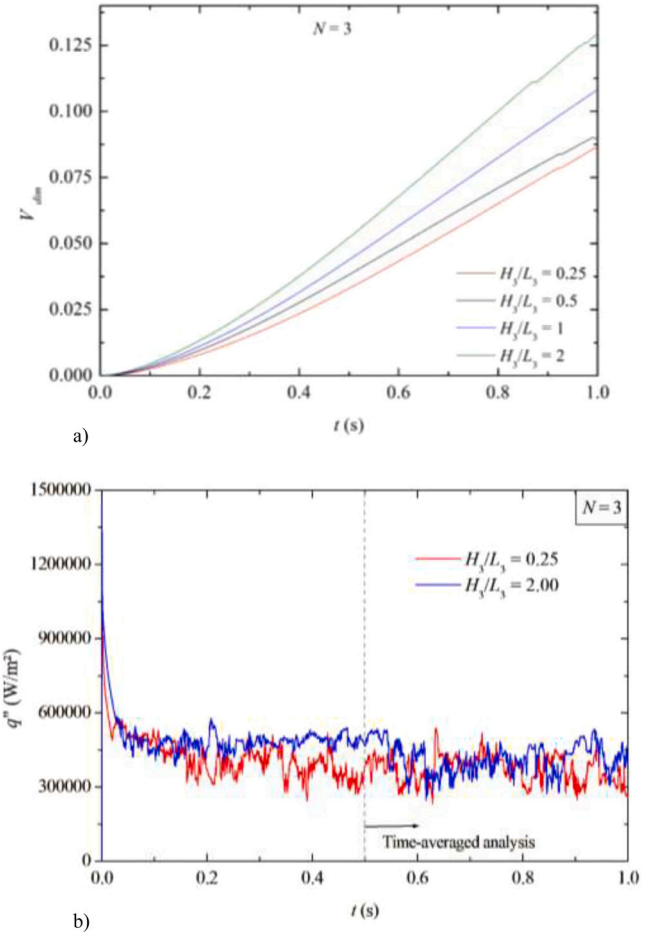

Fig. 13. Instantaneous magnitudes for the configuration with three corrugations ($N = 3$) and different magnitudes of H_i/L_i ($i = 3$): a) dimensionless volume of vapor (V_{dim}), b) heat flux in the lower surface (q'').

length ratio for both corrugations. A similar trend observed for the case with $N = 1$, Fig. 7, is obtained for the configuration with $N = 2$. The differences are the magnitudes of the volume of vapor generated along the time for different ratios of H_2/L_2 and more homogeneous differences

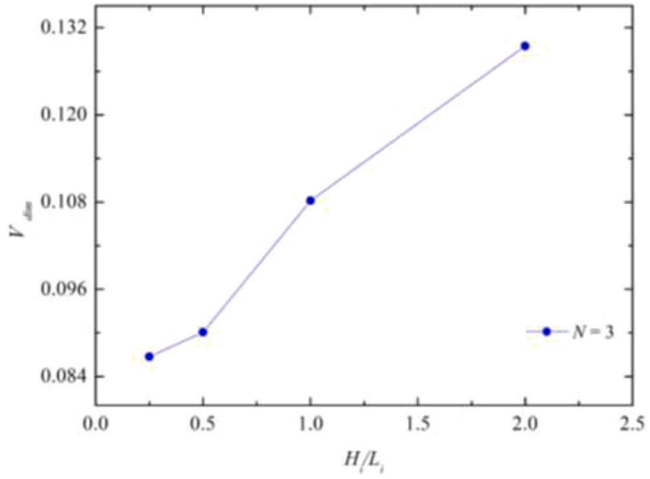

Fig. 14. Effect of the ratio H_i/L_i ($i = 3$) over the dimensionless vapor volume generated in the cavity (V_{dim}) for a cavity with three rectangular corrugations ($N = 3$).

of magnitudes of V_{dim} for different values of H_2/L_2. In general, the magnitudes of V_{dim} increased from $N = 1$ to $N = 2$. For the heat flux (q''), a similar behavior obtained in Fig. 7(b) for $N = 1$ is also reached for $N = 2$, Fig. 10(b). The magnitudes of q'' also stabilized for $t \geq 0.5$ s. However, the time-averaged magnitudes of q'' for $H_2/L_2 = 2.0$ is slightly superior, 0.5 %, than $H_2/L_2 = 0.25$, intensifying even more the difference of heat transfer rate in favor of the case with the highest intrusion.

Similarly to that performed in Fig. 8, Fig. 11 shows the effect of the ratio H_2/L_2 on the V_{dim} for $t = 1.0$ s. It can be noticed again an increase of V_{dim} with the augmentation of the ratio H_2/L_2. Here, for the lowest magnitudes of H_2/L_2, the difference between the $H_2/L_2 = 0.25$ and 0.5 is more pronounced than that reached for the case with $N = 1$. One possible explanation is concerned with the few gaps that the insertion of two corrugations with lowest magnitudes of H_2/L_2 caused among the lateral surfaces of the corrugations and lateral surfaces of the cavity. Fig. 12 illustrates the vapor volume fraction for different magnitudes of H_2/L_2. Fig. 12(a) corroborates the previous observation that the increase of N for lowest ratio of H_2/L_2 conducted to a narrow gap among the corrugations and cavity, generating a vapor film region that acts as thermal insulation. With the augmentation of H_2/L_2, like the behavior noticed for $N = 1$, the size of the vapor bubbles also increases using the

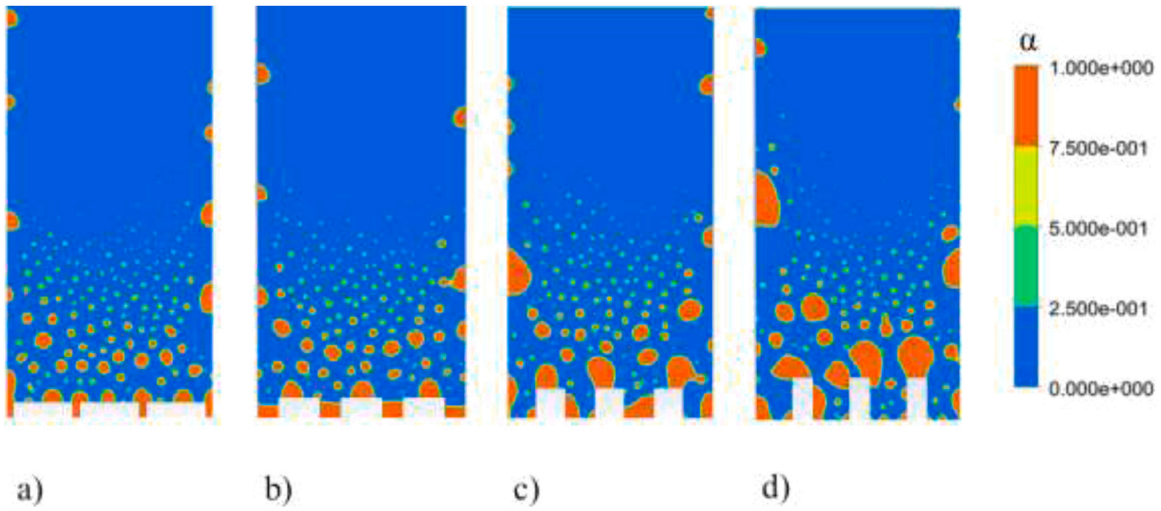

Fig. 15. Volume fraction of vapor generated in the cavity with three corrugations at $t = 1.0$ s for different ratios of H_i/L_i ($i = 3$): a) $H_i/L_i = 0.25$, b) $H_i/L_i = 0.5$, c) $H_i/L_i = 1.0$, d) $H_i/L_i = 2.0$.

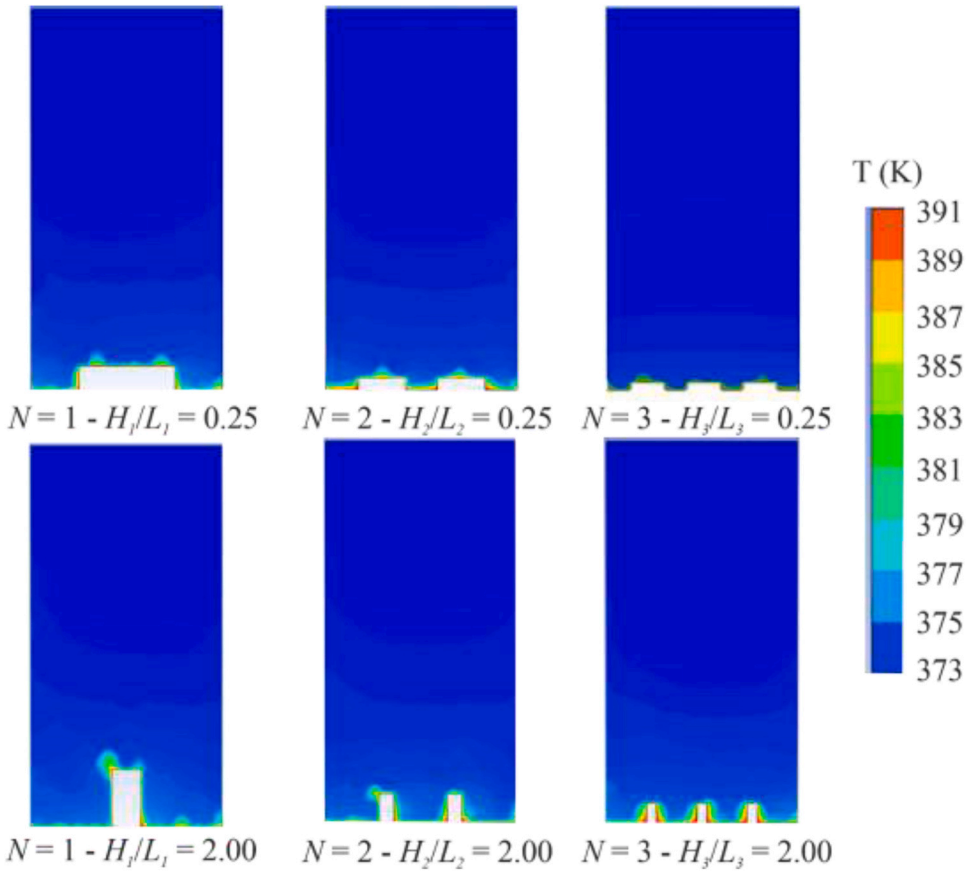

Fig. 16. Temperature field for extreme ratios of H_i/L_i and for different N in the instant of time $t = 1.0$ s.

mechanism previously reported for $N = 1$ (nucleation, integration among different bubbles, increase of bubbles size, detachment in the corrugations and anticipation of bubbly and slug regimes). Here, as depicted in Fig. 12(d), some interaction between some slugs in two different corrugations is noticed.

Fig. 13 illustrates the V_{dim} as a function of time for $N = 3$, Fig. 13(a), and the instantaneous spatial averaged heat flux for the extremes magnitudes of H_3/L_3, Fig. 13(b). Fig. 14 presents the effect of the ratio H_3/L_3 on V_{dim} for $t = 1.0$ s. The behavior is like that noticed for $N = 1$, see Figs. 7 and 8, respectively. Here, the lowest ratios $H_3/L_3 = 0.25$ and 0.5 led to the worst performance due to the formation of vapor regions in the gaps among the corrugations and the lateral surfaces of the cavity, as illustrated in Figs. 15(a) and 15(b). Even in Fig. 15(c), for $H_3/L_3 = 1.0$, the nucleation of bubbles in the gaps interacts in such way as to form some vapor films in this region. For $H_3/L_3 = 2.0$, Fig. 15(d), bubbles of large size detach in slug configuration from each corrugation. In general, results demonstrated that, regardless of the number of corrugations, the lowest magnitudes of H_3/L_3 generated vapor films due to the bubbles

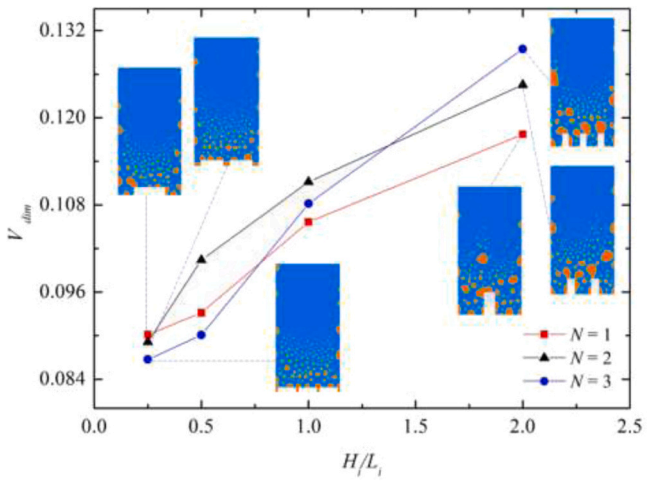

Fig. 17. Comparison of the effect of the ratio H_i/L_i for different numbers of corrugations (N) over the dimensionless volume fraction of vapor (V_{dim}) in the cavity.

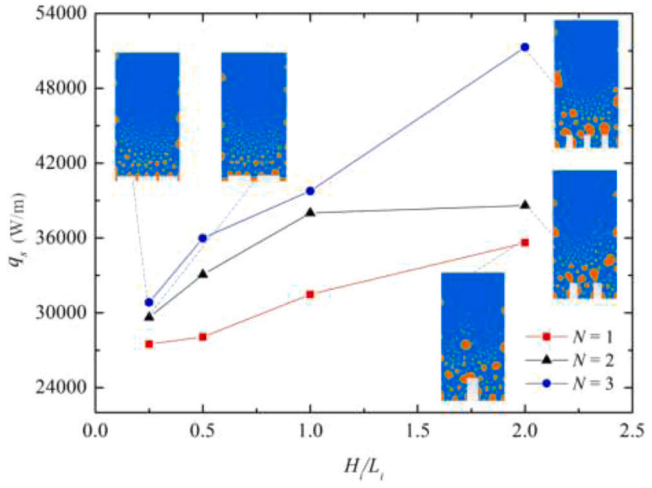

Fig. 18. Comparison of the effect of the ratio H_i/L_i for different numbers of corrugations (N) over the heat transfer rate (q_S) at the inferior surface.

nucleation in the gaps among corrugations and cavities. For the highest magnitudes of H_3/L_3, generated bubbles in the vertical walls of corrugations intensify the scale of generated bubbles, anticipating the bubbly and slug regimes and benefiting the system. Other interesting advantage with the penetration of the corrugations for the present problem is the conducting of higher temperature surfaces further from the basis of the cavity. Fig. 16 illustrates the temperature fields for the extreme magnitudes and different N for $t = 1.0$ s, corroborating the advantage of the intrusion of corrugation in the distribution of thermal fields. Moreover, the slugs generated in each corrugation can interact with each other, increasing the size of the detached vapor structures. Fig. 13(b) shows that q'' for $N = 3$ has similar behavior to that achieved for $N = 1$, Fig. 7 (b), $N = 2$, Fig. 10(b). Here, the performance difference between the cases $H_3/L_3 = 2.0$ and 0.25 increased to around 16 % that associated with the increase of heat exchange area conducted to a significant difference in the heat transfer rate between the extremes for $N = 3$. It is also important to mention that the transient results obtained in the present work for bubble patterns, Figs. 6, 9, 12, and 15, and results for the heat fluxes, Figs. 7(b), 10(b), and 13(b), indicate the achievement of continuous bubble formation, and stabilization of the heat flux in the isothermal surface, which are characteristics of fully developed boiling for all studied cases.

To compare the influence of the height/length ratios of the corrugations for different N, Figs. 17 and 18 show the effect of the ratio H_2/L_2 over V_{dim} and q_s, respectively. In Fig. 17 it is possible to observe that, for low magnitudes of H_2/L_2 the $N = 1$ conducted to a better performance in comparison with $N = 2$ and 3. This behavior is related to the narrow space in the gaps among corrugations and the cavity that generated vapor films in this region, preventing the generation of new bubbles and vapor detachment. For the ratios $H_2/L_2 = 0.5$ and 1.0, the best performance is achieved when $N = 2$, while $N = 3$ is the best only for $H_2/L_2 = 2.0$, i.e., the highest intrusion of the corrugation. In general, results indicated that corrugations with the highest intrusion in the cavity domain and more thinned possible, to prevent the generation of vapor films in corrugations and cavity gaps, conducted a better performance considering the generation of vapor as the performance indicator. The optimal configuration $N_o = 3$ and $(H_2/L_2)_{oo} = 2.0$ led to the formation of multiple-sized vapor structures (slugs, bubbly, and bubbles) associated with the natural convection flow of water from the inferior to upper regions of the cavity, improving the system performance. This case behaved nearly 49 % superior to the worst case with corrugation ($N = 3$ and $H_2/L_2 = 0.25$). For the heat transfer rate per unit length, Fig. 18, contrarily to that seen for V_{dim}, for all ranges of H_2/L_2 the highest number of corrugations conducted to the highest magnitudes of heat transfer rate per unit length (q_s). One explanation for this fact is that, even with the insulation caused by vapor films in the gaps among corrugations and cavities, which is more prominent in the lowest ratios of H_2/L_2, the increase in the number of corrugations increases the heat exchange area between the lower isothermal surface of the cavity and the fluid, compensating the presence of vapor films. For example, the perimeter increases from $per = 50$ mm to 68.28 mm for $N = 1$, $per = 54.14$ mm to 80 mm for $N = 2$, and $per = 55$ mm to 82.43 mm for $N = 3$, when the ratios $H_i/L_i = 0.25$ and 2 are compared. For q_s, the increase in the number of N and H_i/L_i ratios led to the improvement of the thermal performance for all studied configurations. Results also indicated that the bared surface led to a heat transfer rate per unit depth of $q_s = 26{,}675$ W·m^{-1}, which is quite close to the performance reached for the worst configurations with $N = 1$, e.g., for $H_2/L_2 = 0.25$ it is obtained $q_s = 27{,}200$ W·m^{-1}. For the global optimal configuration, $N_o = 3$ and $(H_3/L_3)_{oo} = 2.0$, the heat transfer rate per unit depth is $(q_s)_{mm} = 51{,}300$ W·m^{-1}, which is 1.88 and 1.92 times superior to the worst corrugated case and bared surface.

5. Conclusions

In the present numerical work, it was performed a geometrical investigation of a corrugated isothermal surface placed in a two-dimensional cavity under turbulent pool boiling flows. The geometry is analyzed in light of the constructal design method, investigating the effect of the height/length ratios for three different numbers of corrugations. The cavity and corrugation areas are the constraints and the dimensionless volume of vapor generated (V_{dim}) and heat transfer rate per unit depth (q_s) are the performance indicators.

Firstly, the numerical method used here was validated with the correlation of Rohsenow [42] for the prediction of heat flux and convection heat transfer coefficient for a cavity with a bared isothermal surface and considering one excess of temperature of $\Delta T_e = 18$ °C. It was achieved differences inferior to 7.0 %, which is within the uncertainty of the correlation. Moreover, the nucleation of bubbles, columns, and slugs of vapor generated agreed with the behavior described in the literature for the thermal conditions investigated [13,26,43]. Therefore, the present numerical method was employed for the geometrical investigation of the corrugations in the lower surface of the cavity.

Concerning the geometrical investigation, results demonstrated the insertion of corrugations benefited the system, regardless of the performance indicator (generation of vapor in the cavity or heat transfer rate per unit depth). For example, the q_s obtained for the optimal configuration, $N_o = 3$ and $(H_3/L_3)_{oo} = 2.0$ was almost two times superior

than the case with bared surface. Results recommended avoiding corrugations with the lowest ratios of H_i/L_i, mainly for $N = 2$ and 3, since these configurations can induce the formation of vapor films in the narrow gaps among corrugations and cavity, preventing the generation of slugs and columns of vapor and restricting the vapor generation and heat transfer between the isothermal surface and water flow. To improve the performance, results indicated for the present conditions that corrugations with the highest H_i/L_i and N led to the best thermal performance in terms of V_{dim} and q_s, i.e., thin, and intruded configurations. Moreover, the best configurations were able to allow the generation of large-size vapor slugs and columns of vapor for each corrugation, which interacts with bubbles transported by natural convection and vapor structures generated in other corrugations. In general, the best performance was reached when the multiplicity of scales of vapor structures increased, i.e., few large and many small structures, which agreed with the constructal law distribution that benefits the flow system.

The investigation of other corrugations and conditions for the pool boiling in the cavity flow should be investigated in future works.

CRediT authorship contribution statement

Gabryell Malcher Freire: Visualization, Validation, Software, Data curation. **Cesare Biserni:** Writing – review & editing, Resources. **Claudia Naldi:** Writing – review & editing, Methodology, Investigation, Formal analysis. **Felipe Roman Centeno:** Validation, Software, Data curation. **Liércio André Isoldi:** Visualization, Validation, Data curation. **Luiz Alberto Oliveira Rocha:** Supervision, Funding acquisition. **Cícero Coelho de Escobar:** Validation, Formal analysis, Data curation. **Elizaldo Domingues dos Santos:** Writing – review & editing, Writing – original draft, Supervision, Methodology, Investigation, Conceptualization.

Declaration of competing interest

The authors declare that they have no known competing financial interests or personal relationships that could have appeared to influence the work reported in this paper.

Acknowledgements

The author G. M. Freire thanks the Coordenação de Aperfeiçoamento de Pessoal de Nível Superior (CAPES) – Finance Code 001. Authors L.A. O. Rocha, L.A. Isoldi, and E.D. dos Santos thank CNPq – National Council of Scientific and Technological Development for the research grant (Processes: 307791/2019–0, 309648/2021–1, 308396/2021–9). Authors also thank FAPERGS – Fundação de Apoio à Pesquisa do Estado do Rio Grande do Sul (Grant number: 19/2551–0001847–9). The authors L. A.O. Rocha and E.D. dos Santos also thank Fundação para a Ciência e Tecnologia, I.P. (doi.org/10.54499/UIDP/04683/2020). C. Biserni and C. Naldi are sponsored by the National Recovery and Resilience Plan (NRRP), Mission 4 Component 2 Investment 1.5 - Call for tender No. 3277 of 30/12/2021 of Italian Ministry of University and Research funded by the European Union – NextGenerationEU; project code ECS00000033, Concession Decree No. 1052 of 23/06/2022 adopted by the Italian Ministry of University and Research, CUP D93C22000460001, "Ecosystem for Sustainable Transition in Emilia-Romagna" (Ecosister), Spoke 4.

References

[1] S.G. Kandlikar, Controlling bubble motion over heated surface through evaporation momentum force to enhance pool boiling heat transfer, Appl. Phys. Lett. 102 (2013) 051611, https://doi.org/10.1063/1.4791682.
[2] I. Perez-Raya, S.G. Kandlikar, Evaporation on a planar interface – numerical simulation and theoretical analysis of heat and mass transport processes, Adv. Heat Transf. 48 (2016) 125–190, https://doi.org/10.1016/bs.aiht.2016.08.005.
[3] S.K. Singh, D. Sharma, Review of pool and flow boiling heat transfer enhancement through surface modification, Int. J. Heat Mass Transf. 181 (2021) 122020, https://doi.org/10.1016/j.ijheatmasstransfer.2021.122020.
[4] S. Hong, J. Wang, Z. Gao, C. Dang, Review on state-of-the-art research in pool and flow boiling under microgravity, Exp. Therm. Fluid Sci. 144 (2023) 110848, https://doi.org/10.1016/j.expthermflusci.2023.110848.
[5] S.K. Gupta, R.D. Misra, Effect of two-step electrodeposited Cu–TiO_2 nanocomposite coating on pool boiling heat transfer performance, J. Therm. Anal. Calorim. 136 (4) (2019) 1781–1793, https://doi.org/10.1007/s10973-018-7805-7.
[6] Y. Watanabe, K. Enoki, T. Okawa, Nanoparticle layer detachment and its influence on the heat transfer characteristics in saturated pool boiling of nanofluids, Int. J. Heat Mass Transf. 125 (2018) 171–178, https://doi.org/10.1016/j.ijheatmasstransfer.2018.04.072.
[7] A. Joseph, S. Mohan, C.S. Kumar, A. Mathew, S. Thomas, B.R. Vishnu, S.P. Sivapirakasam, An experimental investigation on pool boiling heat transfer enhancement using sol-gel derived nano-CuO porous coating, Exp. Therm. Fluid Sci. 103 (2019) 37–50, https://doi.org/10.1016/j.expthermflusci.2018.12.033.
[8] L.Y.X. Lum, P. Liu, J.Y. Ho, Micro/nanostructuring of metal additively manufactured aluminum alloy for enhanced pool boiling of dielectric fluids, Int. J. Heat Mass Transf. 221 (2024) 125090, https://doi.org/10.1016/j.ijheatmasstransfer.2023.125090.
[9] Z. Lei, B. Liu, P. Xu, Y. Zhang, J. Wei, The pool boiling heat transfer and critical vapor column coalescence mechanism of block-divided microstructured surfaces, Int. J. Heat Mass Transf. 150 (2020) 119362, https://doi.org/10.1016/j.ijheatmasstransfer.2020.119362.
[10] J. Zhou, P. Xu, B. Qi, Y. Zhang, J. Wei, Effects of micro-pin-fins on the bubble growth and movement of nucleate pool boiling on vertical surfaces, Int. J. Therm. Sci. 171 (2022) 107186, https://doi.org/10.1016/j.ijthermalsci.2021.107186.
[11] J.S. Kim, W. Kim, H.S. Kim, Y. Kim, S.H. Yoon, Pool boiling heat transfer of ammonia outside a single tube with fin structures: Hysteresis phenomena and boiling enhancement, Int. Commun. Heat Mass Transf. 149 (2023) 107157, https://doi.org/10.1016/j.icheatmasstransfer.2023.107157.
[12] Y. Chen, B. Yu, W. Lu, B. Wang, D. Sun, K. Jiao, W. Zhang, W. Tao, Review on numerical simulation of boiling heat transfer from atomistic to mesoscopic and macroscopic scales, Int. J. Heat Mass Transf. 225 (2024) 125396, https://doi.org/10.1016/j.ijheatmasstransfer.2024.125396.
[13] A. Mukherjee, V.K. Dhir, Study of lateral merger of vapor bubbles during nucleate pool boiling, ASME J. Heat Transf. 126 (6) (2004) 1023–1039, https://doi.org/10.1115/1.1834614.
[14] W. Lee, G. Son, Bubble dynamics and heat transfer during nucleate boiling in a microchannel, Numer. Heat Transf. A 53 (10) (2008) 1074–1090, https://doi.org/10.1080/10407780701789898.
[15] G. Tomar, G. Biswas, A. Sharma, A. Agrawal, Numerical simulation of bubble growth in film boiling using a coupled level-set and volume-of-fluid method, Phys. Fluids 17 (2005) 1–13, https://doi.org/10.1063/1.2136357.
[16] Z. Zhao, J. Zhang, D. Jia, K. Zhao, X. Zhang, P. Jiang, Thermal performance analysis of pool boiling on an enhanced surface modified by the combination of microstructures and wetting properties, Appl. Therm. Eng. 117 (2017) 417–426, https://doi.org/10.1016/j.applthermaleng.2017.02.014.
[17] N.K. Singh, B. Premachandran, Numerical investigation of film boiling on a horizontal wavy wall, Int. J. Heat Mass Transf. 150 (2020) 119371, https://doi.org/10.1016/j.ijheatmasstransfer.2020.119371.
[18] S.M. Thamil Kumaran, B. Premachandran, Study of flow and heat transfer characteristics of saturated flow film boiling over two inline cylinders, Phys. Fluids 34 (11) (2022) 112123, https://doi.org/10.1063/5.0125192.
[19] A. Bejan, Shape and structure, from engineering to nature, Cambridge University, Cambridge, UK, 2000.
[20] A. Bejan, S. Lorente, Design With Constructal Theory, John Wiley & Sons, Hoboken, N.J, 2008.
[21] A. Bejan, The physics of life: the evolution of everything, St. Martins Press, New York City, 2016.
[22] E.D. dos Santos, L.A. Isoldi, M.N. Gomes, L.A.O. Rocha, The constructal design applied to renewable energy systems, in: E. Rincón-Mejía, A. de las Heras (Eds.), Sustainable energy technologies, first ed., CRC Press - Taylor & Francis Group, Boca Raton, 2017, pp. 63–87.
[23] P.M. Rodrigues, C. Biserni, C.C. de Escobar, L.A.O. Rocha, L.A. Isoldi, E.D. dos Santos, Geometric optimization of a lid-driven cavity with two rectangular intrusions under mixed convection heat transfer: a numerical investigation motivated by constructal design, Int. Commun. Heat Mass Transf. 117 (2020) 104759, https://doi.org/10.1016/j.icheatmasstransfer.2020.104759.
[24] R.S. Borahel, F.S.F. Zinani, L.A.O. Rocha, E.D. dos Santos, L.A. Isoldi, C. Biserni, Geometric optimization of a rectangular isothermal block inside a lid-driven cavity by means of constructal design, Int. Commun. Heat Mass Transf. 139 (2022) 106499, https://doi.org/10.1016/j.icheatmasstransfer.2022.106499.
[25] R.C. Oliveski, F. Becker, L.A.O. Rocha, C. Biserni, G.E.S. Eberhardt, Design of fin structures for phase change material (PCM) melting process in rectangular cavities, J. Energy Storage 35 (2021) 102337, https://doi.org/10.1016/j.est.2021.102337.
[26] D. Sun, J. Xu, Q. Chen, Modeling of the evaporation and Condensation phase-change problems with FLUENT, Numer. Heat Transf. 66 (2014) 326–342, https://doi.org/10.1080/10407790.2014.915681.
[27] A. Bejan, Convection Heat Transfer, fourth ed., Wiley, Hoboken, New Jersey, 2013.
[28] B.J. Mcbride, S.D. Gordon, M.A. Reno, Coefficients for calculating thermodynamic and transport properties of individual species, NASA Techn. Memorand. 4513 (1993).
[29] D.C. Wilcox, Turbulence Modeling for CFD, third ed., DCW Industries, 2006.

[30] B.E. Launder, D.B. Spalding, The numerical computation of turbulent flows, Comput. Methods Appl. Mech. Eng. 3 (1974) 269–289.
[31] H.L. Wu, X.F. Peng, P. Ye, Y.Eric Gong, Simulation of refrigerant flow boiling in serpentine tubes, Int. J. Heat Mass Transf. 50 (2007) 1186–1195, https://doi.org/10.1016/j.ijheatmasstransfer.2006.10.013.
[32] S.C.K. De Schepper, G.J. Heynderickx, S.C.K. Schepper, G.B. Marin, Modeling the evaporation of a hydrocarbon feedstock in the convection section of a steam cracker, Comput. Chem. Eng. 33 (2009) 122–132, https://doi.org/10.1016/j.compchemeng.2008.07.013.
[33] R. Zhang, T. Cong, W. Tian, S. Qiu, G. Su, Effects of turbulence models on forced convection subcooled boiling in vertical pipe, Ann. Nucl. Energy 80 (2015) 293–302, https://doi.org/10.1016/j.anucene.2015.01.039.
[34] C.W. Hirt, B.D. Nichols, Volume of fluid (VOF) method for the dynamics of free boundaries, J. Comput. Phys. 39 (1981) 201–225, https://doi.org/10.1016/0021-9991(81)90145-5.
[35] W.H. Lee, A pressure iteration scheme for two-phase flow modeling, in: T. N. Veziroglu (Ed.), Multiphase Transport Fundamentals, Reactor Safety, Applications, Hemisphere, Washington, DC, 1980.
[36] C.R. Machado, F.A.D. Cabral, *Metodologia De Análise Numérica Do Processo De Ebulição Em Piscina No Evaporador De Um Termossifão Fechado* (In portuguese). Monography of Conclusion Work in Mechanical Engineering, Universidade Tecnológica Federal do Paraná, Curitiba, 2017.
[37] V. Srinivasan, A.J. Salazar, K. Saito, Modeling the disintegration of modulated liquid jets using volume-of-fluid (VOF) methodology, Appl. Math. Model. 35 (2011) 3710–3730, https://doi.org/10.1016/j.apm.2011.01.040.
[38] J.U. Brackbill, D.B. Kothe, C. Zemach, A continuum method for modeling surface tension, J. Comput. Phys. 100 (1992) 335–354, https://doi.org/10.1016/0021-9991(92)90240-Y.
[39] S.V. Patankar, Numerical heat transfer and fluid flow, McGraw-Hill, New York, USA, 1980.
[40] H.K. Versteeg, W. Malalasekera, An introduction to computational fluid dynamics: the finite volume method, Pearson Education Limited, London, UK, 2007.
[41] ANSYS. FLUENT User's Guide, Version 14.0; ANSYS Inc.: Canonsburg, PA, USA, 2011.
[42] W.M. Rohsenow, A method for correlating heat transfer data for surface boiling of liquids, Trans. ASME 74 (1952) 969–976, https://doi.org/10.1115/1.4015984.
[43] G. Son, V.K. Dhir, Dynamics and heat transfer associated with a single bubble during nucleate boiling on a horizontal surface, J. Heat Transf. 121 (1999) 623–631, https://doi.org/10.1115/1.2826025.